AIChE WILEY InterScience DISCOVER SOMETHING GREAT

MATERIALS, INTERFACES AND ELECTROCHEMICAL PHENOMENA

A Kinetic Study of Vesicle Fusion on Silicon Dioxide Surfaces by Ellipsometry

Dimitrios Stroumpoulis, Alejandro Parra, and Matthew Tirrell
Dept. of Chemical Engineering and Materials Research Laboratory, University of California at Santa Barbara, Santa Barbara, CA 93106

DOI 10.1002/aic.10914
Published online June 9, 2006 in Wiley InterScience (www.interscience.wiley.com).

Ellipsometry and a mass transport model were used to investigate the kinetics of lipid bilayer formation on silicon dioxide surfaces from 100 nm diameter 1,2-dimyristoyl-sn-glycero-3-phosphocholine (DMPC) vesicles. For the range of concentrations studied, 0.025 to 0.380 mg/mL, the rate of the process was found to be concentration dependent and adsorption limited. Further experiments, particularly at concentrations > 0.380 mg/mL, presented evidence of net mass desorption as an intermediate step to supported lipid bilayer formation. © 2006 American Institute of Chemical Engineers *AIChE J,* 52: 2931–2937, 2006
Keywords: vesicle fusion, bilayers, kinetic study, ellipsometry, desorption

Introduction

Supported lipid bilayers (SLBs) and techniques to form them in a consistent and controlled fashion will become necessary to the extent that microscale-level devices are developed for various technological applications.[1] SLBs are a good platform for surface functionalization, given that transmembrane proteins and peptides[2] can be incorporated in a biologically relevant environment with control over their concentration, presentation, and lateral mobility. Lab-on-a-chip devices, enabled by recent advances in lithography and microfluidics, demand the development of new nanofabrication techniques.[3] A promising strategy is to use bottom-up processes driven by molecular assembly,[4] such as the formation of SLBs from vesicle solutions. A basic understanding of such phenomena is essential to foresee their possible applications and limitations.

Vesicle fusion is a convenient method for creating SLBs on both flat and textured topologies. This is an advantage with respect to the Langmuir–Blodgett deposition technique, which can be effective only on flat surfaces. Additional advantages are the simplicity of the process and the ability to control its rate. Vesicle fusion also offers the possibility of surface functionalization using composition gradients.[5] Such gradients could serve as a valuable tool in assessing the ability of bioactive species in multicomponent membranes to modify cell function (that is, adhesion[6] or migration[7]).

There has been a significant amount of experimental work on vesicle fusion by Kasemo and coworkers using the quartz crystal microbalance-dissipation (QCM-D) technique.[8] It was concluded that vesicles adsorb irreversibly on SiO_2, Si_3N_4, TiO_2, oxidized Pt, and oxidized Au surfaces. However, vesicle to bilayer transformation occurs only in the first two cases, whereas in the other cases the vesicles remain intact but are deformed. The extent of deformation of vesicles on SiO_2 has been found to be greater than that on TiO_2, which is thought to arise from a stronger attraction to the surface. In both cases larger vesicles are more deformed than smaller ones by the surface interaction. The different polarizabilities and isoelectric points of the above-mentioned surfaces are important parameters governing the strength of the van der Waals and electrostatic interactions between the vesicles and the surface.

Similar experiments[8] have demonstrated that there is a critical vesicle coverage required for rupture to commence, irrespective of vesicle size. This is inconsistent with a mechanism requiring vesicles to fuse with each other on the surface until a critical radius for rupture to take place is reached because, if that were true, large vesicles would fuse immediately. This critical vesicle coverage, instead, suggests that vesicle–vesicle interactions are required to enhance vesicle deformation and induce rupture.

Correspondence concerning this article should be addressed to D. Stroumpoulis at dimitris@engineering.ucsb.edu.

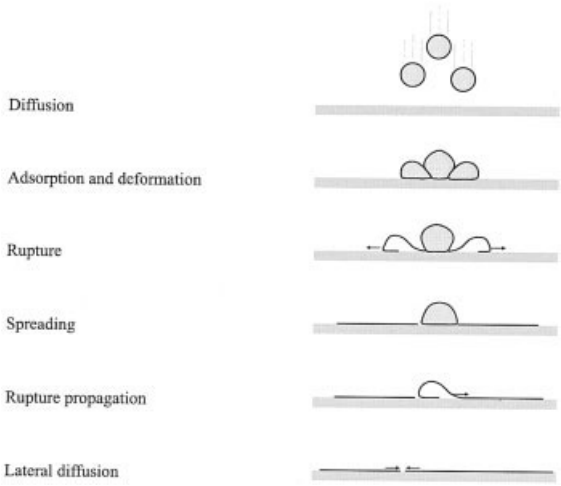

Figure 1. Possible mechanism of vesicle fusion on hydrophilic surfaces.

Vesicles diffuse from the bulk to the surface, where adsorption begins and proceeds until a critical concentration of adsorbed vesicle mass is reached. Vesicles rupture and begin to spread on the surface, whereas adsorbed bilayer fragments propagate the formation of pores on unruptured vesicles. The process is completed by the lateral diffusion of bilayer fragments to minimize the hydrophobic edge energy.

The vesicle is most likely to rupture at the point where the radius of curvature is the smallest. At this point deformation, caused by adhesion to the surface and interaction between vesicles, increases the lateral tension (Σ) within the membrane. In principle,[9] the formation of a pore can reduce the vesicle's energy, given that a pore of radius L within a planar membrane has energy $F_{\text{pore}} = 2\pi L\Sigma_e - \pi L^2\Sigma$, where Σ_e is the line tension arising from the hydrophobic edge. Once a pore is formed its radius (L) will tend to increase until the lateral tension in the membrane (Σ) is relieved, such that equilibrium is reached ($dF_{\text{pore}}/dL = 0$).

The vesicle to bilayer transition has been shown to be thermally activated[8] in that the critical vesicle coverage required for rupture is inversely proportional to temperature. Bilayer formation can be prevented by adsorption at sufficiently low temperature (that is, below the lipid chain melting temperature). Outward osmotic gradients also favor rupture, by causing compressive stresses on the vesicles. On the other hand, an inverse gradient has a weaker effect on rupture. An important conclusion that has been drawn from fusion experiments with proteoliposomes is that the inner surface of the vesicle becomes the leaflet of the bilayer facing the surface.[10]

Given the aforementioned experimental observations the possible mechanism of vesicle fusion on hydrophilic surfaces is summarized in Figure 1. Vesicles initially diffuse from the bulk to the surface, where adsorption begins and proceeds until a critical concentration of adsorbed vesicle mass is reached. This requirement possibly reflects the existence of a vesicle deformation threshold, which is reached by vesicle–surface and vesicle–vesicle interactions. The small radius of curvature at the point that the vesicles curve away from the surface initiates a mechanism of pore formation. The ruptured vesicles begin to spread on the surface, where they adsorb. Adsorbed bilayer fragments propagate the formation of pores on unruptured vesicles by the "catalytic" action of hydrophobic edges, just as preruptured vesicles are believed to catalyze vesicle fusion.[11] The process is completed by the lateral diffusion of bilayer fragments to minimize the hydrophobic edge energy.

Techniques that have been used to study the formation of SLBs by vesicle fusion include surface plasmon resonance,[12,13] neutron reflectivity,[14] atomic force microscopy,[15,16] confocal fluorescence correlation spectroscopy, and nulling ellipsometry.[17] In these studies, there have rarely been any attempts to look at the kinetics of the process while making an effort to interpret the results in terms of mass transport models.[18,19] Such models, commonly used in chemical engineering applications, are important to the extent that they can give a quantitative and qualitative understanding of the process under investigation. Computer simulations of the formation of SLBs from vesicle solutions can give insight into the process, but these are also rare.[20]

In the present study, we observe SLB formation from vesicle solutions on hydrophilic silicon dioxide substrates with the optical technique of phase-modulated ellipsometry and the results are interpreted in conjunction with a mass transport model.[19]

Experimental

Materials and methods

Small unilamellar vesicle (SUV) solutions were prepared from 1,2-dimyristoyl-sn-glycero-3-phosphocholine (DMPC) purchased from Avanti Polar Lipids (Alabaster, AL). The lipids were dissolved in chloroform and a thin film was formed on the walls of a glass test tube by nitrogen-flow–induced evaporation. The sample was left overnight in a vacuum chamber to ensure complete removal of the solvent. The lipids were then reconstituted in Millipore water (18 MΩcm), briefly vortexed, and left to hydrate in a 37°C water bath for 1 h. The multilamellar vesicle solution thus formed was extruded five times through a polycarbonate membrane filter (100 nm nominal pore size) in a temperature-controlled extruder at 40°C. Dynamic light scattering was used to confirm the formation of vesicles with a monodisperse diameter distribution $\simeq$ 100 nm. The extruded solutions were kept at 5°C and used within a week.

Polished silicon wafers, with a native oxide layer about 15 Å thick, were treated in piranha solution (70% H_2SO_4, 30% H_2O_2 v/v) for 30 min, briefly rinsed in Millipore water, and quickly placed in a 20 mL cylindrical quartz cell filled with water. The cell was subsequently fastened onto the stage of a phase-modulated picometer ellipsometer (Beaglehole Instruments, Wellington, New Zealand) and rapidly fed with 10 mL of a vesicle solution of the desired concentration, displacing an equal volume of water. Ellipsometric measurements were taken at the Brewster angle of incidence for the silicon–water interface (71°) using the 632.8 nm line from a He–Ne laser. Kinetic data were collected at 25°C for 1 h after injection, with a time interval of 1 s.

Ellipsometric data analysis

The Fresnel reflection coefficients of an interface are given by

$$r_p = \frac{|E_p^r|}{|E_p^i|} e^{i(\varepsilon_p^r - \varepsilon_p^i)} \tag{1}$$

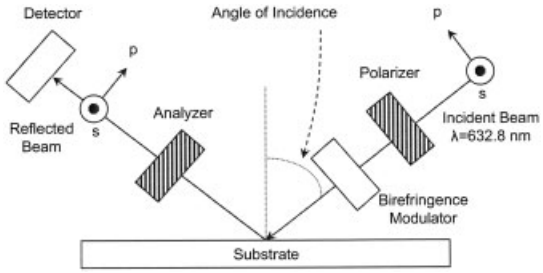

Figure 2. Experimental setup of the phase-modulated ellipsometer.

$$r_s = \frac{|E_s^r|}{|E_s^i|} e^{i(\varepsilon_s^r - \varepsilon_s^i)} \tag{2}$$

where $E_{p,s}^{i,r}$ is the electric field amplitude and $\varepsilon_{p,s}^{i,r}$ is the phase of the beam before and after reflection, in the p (parallel to the plane of incidence) or s (perpendicular to the plane of incidence) polarization (Figure 2).

The ratio of the complex Fresnel reflection coefficients is defined as

$$r = \frac{r_p}{r_s} = \mathrm{Re}(r) + i\,\mathrm{Im}(r) \tag{3}$$

The measured quantity y is given by the following equation:

$$y = \mathrm{Im}(r)\frac{2}{1 + \mathrm{Re}^2(r) + \mathrm{Im}^2(r)} \tag{4}$$

Equation 4 can be simplified under the following conditions: (1) the measurements are performed at the pseudo-Brewster angle of the system, which for nonabsorbing films implies that $\mathrm{Re}(r) = 0$, and (2) the measured values (y_{final} and $y_{initial}$) are positive and small (<0.1), which implies that the corresponding $\mathrm{Im}(r)$ values are also small (<0.1). After applying these simplifications to Eq. 4 we obtain

$$\Delta y = 2\Delta\ \mathrm{Im}(r) \tag{5}$$

Δy can be related to the film thickness (d) through[21]

$$\Delta y = \frac{2\pi\sqrt{n_1^2 + n_2^2}}{\lambda(n_1^2 - n_2^2)}\frac{(n^2 - n_1^2)(n^2 - n_2^2)}{n^2}d \tag{6}$$

where n_1, n_2, and n are the refractive indices of the solvent, the substrate, and the film, respectively, assuming an isotropic refractive index for the film.

Mass Transport Model

The mass transport model used to describe the diffusion–adsorption problem in a stationary fluid is given by the following set of equations[22]:

$$\frac{\partial C(z,t)}{\partial t} = D\frac{\partial^2 c(z,t)}{\partial z^2}$$

$$\frac{d\Gamma}{dt} = D\left.\frac{\partial C}{\partial z}\right|_{z=0} = K\left(1 - \frac{\Gamma}{\Gamma_m}\right)C|_{z=0}$$
$$C|_{z\to\infty} = C_0 \qquad C|_{t=0} = C_0 \qquad \Gamma|_{t=0} = 0 \tag{7}$$

where C is the concentration, Γ is the surface coverage, D is the diffusion coefficient, K is the adsorption rate constant, and Γ_m is the maximum surface concentration. By substituting $\theta = \Gamma/\Gamma_m$, Eq. 7 can be written as a partial differential equation with a nonlinear boundary condition and an ordinary differential equation (ODE):

$$\frac{\partial C(z,t)}{\partial t} = D\frac{\partial^2 C(z,t)}{\partial z^2}$$
$$D\left.\frac{\partial C}{\partial z}\right|_{z=0} = K(1-\theta)C|_{z=0}$$
$$C|_{z\to\infty} = C_0 \qquad C|_{t=0} = C_0 \tag{8}$$

and

$$\frac{d\theta}{dt} = \frac{K}{\Gamma_m}(1-\theta)C|_{z=0}$$
$$\theta|_{t=0} = 0 \tag{9}$$

The finite difference method was applied to discretize Eqs. 8 and 9: $dC^k dt = D\,C^{k+1} + C^{k-1} - 2C^k \Delta z \cdot \Delta z \qquad k = 1, 2, , N-1$

$$\frac{d\theta}{dt} = \frac{K}{\Gamma_m}(1-\theta)C^1 \tag{10}$$

as well as their boundary conditions:

$$D\frac{C^2 - C^0}{2\Delta z} = \frac{C^N - C_0}{k(1-\theta)C^1} \tag{11}$$

where N is the number of cells in the space grid and Δz is the cell size. By setting N to 2000 and Δz to 0.02 cm, Eqs. 10 and 11 can be solved numerically using an ODE solver.

The mass transport model defined by Eq. 7 was developed for a stationary fluid. Under the experimental conditions found here and as discussed later in this article, initial convective effects can influence the value of the diffusion coefficient. We will therefore be estimating an effective diffusion coefficient D. Furthermore, because of the complexity of the vesicle fusion mechanism, it is likely that partial or complete desorption of vesicles is an intermediate step in the reorganization of adsorbed vesicles into bilayer fragments. Therefore, the adsorption rate constant K represents the net adsorption of mass to the surface.

Results and Discussion

Thickness and coverage estimation

The observed values of the experimental quantity y were always <0.1. These values are sufficiently small to make Eq. 5 a valid approximation of Eq. 4. Substitution of the experimental values of Δy (always in the range of 0.032 to 0.034) along with the refractive indices for silicon (3.88) and water (1.33) leaves two values in Eq. 6 undefined: the film thickness d and its refractive index n.

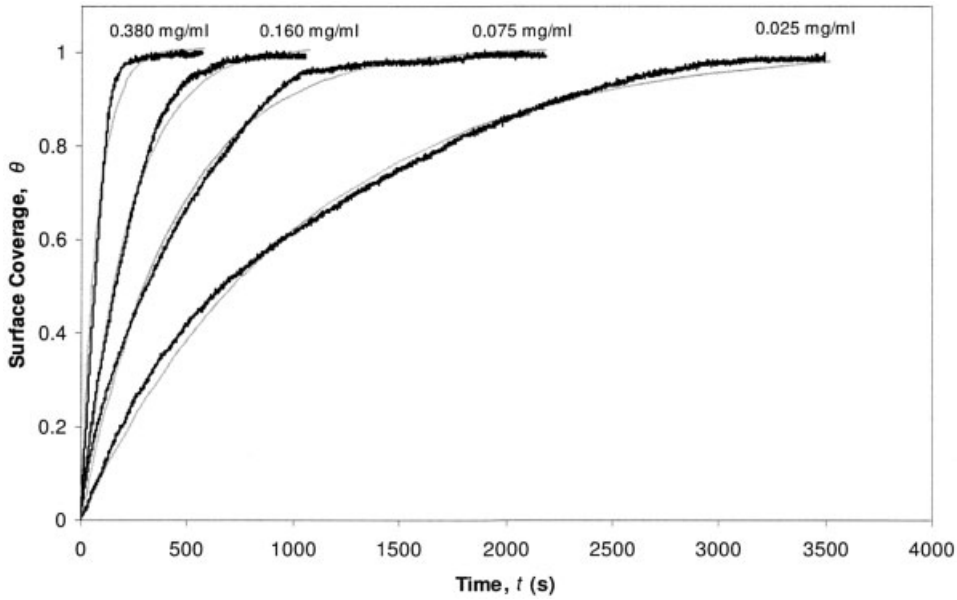

Figure 3. SLB formation kinetics for fusion of DMPC vesicles onto SiO_2 surfaces.

Experimental data (dark lines) and fitting of the numerical solution to the mass transport model (light lines).

The refractive index of DMPC lipid molecules assembled in a bilayer is not known because it might be different from that in solution.[21] As an approximation it is reasonable to expect it to be in the same range as the refractive index of a fatty acid film of similar thickness. Using the refractive index[21] of a monolayer of fatty acids with twice the chain length of DMPC ($n = 1.48$) results in a thickness of 43.5 Å, which is close to the expected value for a single DMPC bilayer (~44.5 Å for DMPC vesicles[23]). A more elaborate model[24] that incorporates the native SiO_2 layer on top of silicon (measured 15 Å), the water layer[25] (~10 Å) trapped between the bilayer and SiO_2 as well as the imaginary part of the refractive index of silicon ($k_r = 0.018$) was also applied to produce a very similar result ($d = 43.1$ Å). On this basis, it was assumed that the final surface coverage in all experiments was 100%. Given that the headgroup area for DMPC is known[26] to be 59 $Å^2$, the maximum surface coverage is 3.8 mg/m^2, and this value was used to scale all the experimental data.

An important assumption in the analysis is that the ellipsometric signal y is proportional to the amount of mass on the surface. Although this is probably true for mass of similar structure (that is, vesicles) it might not be the case during the fusion process because, in principle, vesicles and bilayer fragments can have different optical properties. In this study the average thickness of dry mass on the surface at time t was calculated using Eq. 6, assuming that the refractive index of lipids in vesicles, planar bilayers, and intermediate structures has the same value.

Kinetic analysis

The fitting of the numerical solution of the mass transport model to the experimental data is presented in Figure 3. It can be readily seen that the rate of the process increases with the lipid concentration in the bulk and that a good fit is achieved in all cases. However, in contrast to the QCM-D[8] signal, there is no local maximum in the surface concentration curve and therefore no apparent critical concentration required for rupture to begin. This is explained by the inability of ellipsometry to detect water mass trapped inside the vesicles.

Table 1 summarizes the values of the fitting parameters K and D. We expect the adsorption rate constant to be independent of concentration and indeed it varies only negligibly, indicating that a simple model can be used to describe this process. It is interesting to note that the effective diffusion coefficient increases with concentration and is orders of magnitude greater than the value predicted by the Stokes–Einstein equation (5.0×10^{-8} cm^2/s for vesicles of 100 nm diameter). The partial deformation caused by the elasticity of DMPC vesicles cannot account for the observed discrepancy. In fact, dynamic light scattering affirms that the Stokes–Einstein equation holds for vesicles, given that the apparent vesicle diameter calculated from the measured diffusion coefficient matches the value expected for vesicles extruded through a 100 nm pore membrane.

This discrepancy can be explained by the uncontrolled mixing conditions generated by the rapid injection of vesicles into the sample cell. More specifically, 10 mL of vesicle solution is injected within 2 s, through a 3 mm inlet, into a cylindrical quartz cell, measuring 2.5 cm in diameter and 5 cm in length, displacing an equal volume of water. This results in complete

Table 1. Estimated Parameter Values for the Fitting of the Mass Transport Model, Eq. 7, to the Experimental Data for DMPC Vesicle Fusion onto SiO_2 Surfaces

Lipid Concentration C_0 (mg/mL)	Adsorption Rate Constant K (cm/s)	Effective Diffusion Coefficient D (cm^2/s)
0.380	1.3×10^{-5}	2.0×10^{2}
0.160	1.1×10^{-5}	2.0×10^{2}
0.075	1.2×10^{-5}	1.2×10^{-3}
0.025	1.6×10^{-5}	8.7×10^{-6}

Table 2. Sensitivity of the Numerical Solution to the Mass Transport Model to Parameters K and D*

	Lipid Concentration C_0 (mg/mL)			
	0.380	0.160	0.075	0.025
Using D from Table 1				
S_K	1.0E-01	9.1E-02	1.2E-01	1.2E-01
S_D	5.0E-06	2.9E-04	3.9E-05	7.9E-04
Using D from Stokes–Einstein equation				
S_K	1.1E-01	1.2E-01	1.2E-01	7.4E-02
S_D	8.4E-08	4.0E-06	9.8E-05	4.3E-03

*The sensitivities were calculated by perturbing the values of K and D by +10%. Initial values for K were obtained from Table 1 and for D from Table 1 or from the Stokes–Einstein equation.

mixing within a couple of seconds, as evident from the uniform diffraction of the laser beam on its path toward and away from the substrate. An upper limit of the time required for convective effects to decay can be estimated using the following expression:

$$t_{\text{decay}} = \frac{l^2}{\nu} \tag{12}$$

where l is the characteristic length scale of the sample cell and ν is the kinematic viscosity of the solution. The actual decay time though is expected to be smaller because of wall friction. By substituting $l = 5$ cm and $\nu = 0.9 \times 10^{-2}$ cm^2/s (water at 25°C) we obtain $t_{\text{decay}} \simeq 46$ min. This time is sufficiently long for convective transport to affect all experiments, but especially those conducted at the higher concentrations. Indeed Table 1 shows that the effective diffusion coefficient decreases with decreasing concentration, probably approaching the Stokes–Einstein value at very small concentrations (in the dilute limit).

The uncontrolled flow field created by the complex geometry of the ellipsometric cell is very difficult to model. Simple unidirectional flow is insufficient to describe the mixing conditions. In the current model the mixing rate is represented by the effective diffusion coefficient, which we believe also accounts for the transient convective effects. The effective diffusion coefficient then represents a weighted average of Stokes–Einstein diffusive mixing and convective mixing. Convection does not affect the adsorption rate constant, which was found to be independent of concentration, as expected. An estimate of the initial value of the effective diffusion coefficient can be obtained by the following equation:

$$D_0 \simeq V_0 l \tag{13}$$

where V_0 is the velocity of the injection stream. By substituting $V_0 \simeq 70$ cm/s we obtain $D_0 \simeq 350$ cm^2/s, which is comparable to the value of D obtained experimentally for the higher concentrations (Table 1).

The sensitivity analysis for parameters K and D in the mass transport model is presented in Table 2. We define the sensitivity of the numerical solution of Eq. 7 to a parameter P as

$$S_P = \frac{dS}{dP} P = \frac{\sum_t (\theta_2 - \theta_1)^2}{P_2 - P_1} P_1 \tag{14}$$

where P is either K or D; θ_1 is the surface coverage at time t, calculated using the optimal parameter value P_1 (given in Table 1); and θ_2 is the surface coverage at time t, calculated by setting the parameter value $P_2 = 1.1P_1$. For the range of concentrations studied, the sensitivity to the adsorption rate constant K is at least two orders of magnitude greater than the sensitivity to the effective diffusion coefficient D (Table 2). Therefore it appears that the rate-limiting step of the process is adsorption, as opposed to diffusion. Given that the value of D is overestimated as the result of convection, the process could very well be diffusion limited. However, this is probably not the case, as can be seen by setting the effective diffusion coefficient equal to the value predicted by the Stokes–Einstein equation and calculating the sensitivities for the new set of parameters (Table 2). Again the sensitivity of the surface coverage to the adsorption rate constant is significantly higher than that to the diffusion coefficient.

Hubbard and coworkers[19] used quasi-elastic light scattering (QELS) and applied a similar kinetic model to obtain values of D close to the Stokes–Einstein value for 100 nm DMPC vesicles fusing onto hydrophobic alkanethiol surfaces. In contrast to the results presented here, they found that the process was diffusion limited for the same range of concentrations. Similar conclusions were drawn by Lingler and coworkers.[27] The explanation may be that a hydrophobic surface catalyzes fusion in the same way that a preruptured vesicle[11] or a bilayer disk does, leading to a faster adsorption rate. Indeed QCM-D experiments[28] have shown that egg phosphatidylcholine (EggPC) vesicles fuse onto alkanethiol monolayers without a critical intact vesicle concentration required for rupture as on SiO_2 surfaces. In addition, the mechanism of this process is different in that a single monolayer, rather than a bilayer, is formed. Other studies have suggested that SLB formation is diffusion limited when 25 nm diameter EggPC vesicles at a lower concentration are used.[13] However, because EggPC has a lower chain melting temperature than that of DMPC used in this study, vesicle rupture would have been facilitated.[8] Further, we emphasize that the conclusions drawn there are more qualitative than quantitative, given that a kinetic model was not used to interpret the data.

Evidence of desorption

Figure 1 shows a monotonic increase in the ellipsometric signal with time until saturation. However, a more interesting trend was observed, especially at higher concentrations. Figure 4 illustrates the variation of the ellipsometric quantity y with time at two different bulk lipid concentrations, one at $C_0 = 0.250$ mg/mL and the other at $C_0 = 0.450$ mg/mL. In both cases, mass adsorbs on the surface up to a maximum value and then the signal gradually decreases to a saturation level that corresponds to a single bilayer, although the maximum y value is considerably higher for $C_0 = 0.450$ mg/mL. Furthermore, whereas the transition from the maximum signal value to the saturation level is smooth for the lower concentration experiment, the curve is quite rough for the higher concentration one, involving multiple local maxima and minima.

These data clearly suggest that mass partially desorbs from the surface before the formation of an SLB. Furthermore, it appears that more mass desorbs at higher concentrations. This trend can be explained by referring to the mechanism outlined

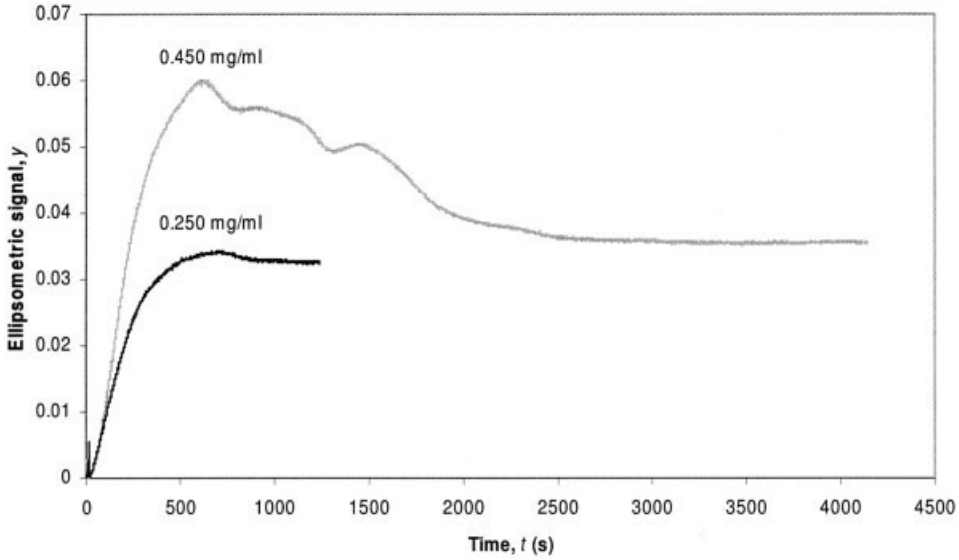

Figure 4. Evidence of mass desorption as an intermediate step to SLB formation.

The ellipsometric signal increases to a maximum value and then gradually decreases to a saturation level that corresponds to a single bilayer.

in Figure 1. Initially, intact vesicles adsorb until a critical concentration is reached for rupture to begin. At sufficiently high concentrations, the rate at which vesicles rupture can be significantly lower than the rate at which they adsorb. In that case, more vesicles will adsorb on the surface than the number required to form one complete bilayer and thus the excess vesicles have to be desorbed. It is expected that a vesicle would be easier to desorb than a bilayer fragment because the ratio of contact area to mass favors the latter. One possible mechanism of intact vesicle desorption is depicted in Figure 5. A ruptured vesicle could insert itself under an intact vesicle, gradually decreasing its contact area and forcing the intact vesicle off the surface. The shape of the curve is consistent with local surface pressure buildup, as vesicles rupture and spread (Figures 5b, 5c, and 5d), and subsequent decrease, as vesicles desorb and more membrane fragments occupy the surface (Figure 5e). A burst of vesicle desorption could be followed by partial vesicle readsorption, if the free surface area generated is larger than the area required by the spreading membrane.

It is possible that this intact vesicle desorption process is not perfect and that some vesicles might be incorporated in the SLB formed, especially at higher concentrations. Indeed, the saturation level at $C_0 = 0.450$ mg/mL (0.035) is slightly higher than the expected value (0.032–0.034). Further, the roughness of the desorption curve at the higher concentration suggests that desorption is not spontaneous. In fact, desorption appears to be the limiting step here, given that more time is required to form a complete bilayer than at lower concentrations (Figure 3). Finally, it is important to note that net mass desorption at C_0 concentrations of $\leq$0.250 mg/mL was only rarely observed, whereas it was always the case at high concentrations ($>$0.450 mg/mL). To our knowledge, this is the first time direct evidence of net mass desorption as an intermediate step to SLB formation has been reported in the literature.

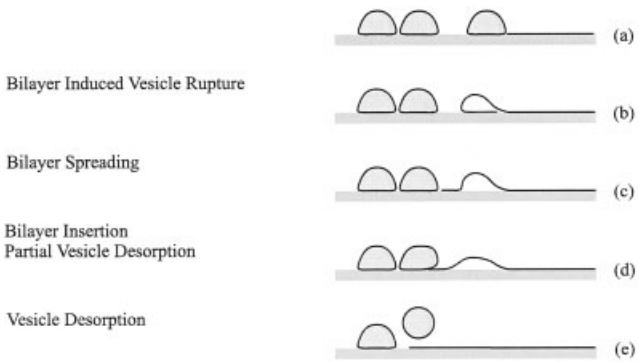

Figure 5. Possible vesicle desorption mechanism.

A ruptured vesicle inserts itself under an intact vesicle, gradually decreasing its contact area and forcing the intact vesicle off the surface.

Conclusions

Ellipsometry was used to monitor the formation of SLBs on silicon dioxide surfaces by vesicle fusion. A mass transport model was applied to investigate the kinetics of the process, which was found to be adsorption limited for the range of concentrations studied. The discrepancy between the effective diffusion coefficient value calculated by the model and that predicted by the Stokes–Einstein equation is believed to be explained by the initial convective effects generated by the rapid injection of vesicles into the sample cell. Further, there was evidence of net mass desorption as an intermediate step to SLB formation, especially at high concentrations.

Clearly, the results presented here embody a more elaborate mechanism for vesicle fusion than what is contained in the model represented by Eq. 7. A companion article[29] attempts to test some of the mechanistic ideas of this discussion by computer simulation.

Acknowledgments

This work was partially supported by the MRSEC Program of the National Science Foundation under Award No. DMR00-80034, the National Science Foundation NIRT Award No. CTS-0103516, the ITR program of the National

Science Foundation under award No. ACI00-86061, and the Army Research Office through the Institute for Collaborative Biotechnologies. The authors thank Badriprasad Ananthanarayanan, Zheming Zheng, and Professor Jacob Israelachvili at UC Santa Barbara and Professor UT Sundararaj at the University of Alberta for their useful comments.

Notation

C = concentration of lipids, mg/mL
C_0 = bulk concentration of lipids, mg/mL
d = film thickness, nm
D = effective diffusion coefficient of mass, cm^2/s
D_0 = initial effective diffusion coefficient of mass, cm^2/s
E_p^r = electric field component of the reflected wave parallel to the plane of incidence
E_p^i = electric field component of the incident wave parallel to the plane of incidence
E_{sp}^r = electric field component of the reflected wave perpendicular to the plane of incidence
E_s^i = electric field component of the incident wave perpendicular to the plane of incidence
F_{pore} = energy of vesicle pore formation, J
J = mass flux, mg cm^{-2} s^{-1}
k_r = imaginary part of the refractive index of silicon
K = adsorption rate constant, cm/s
L = vesicle pore radius, nm
l = characteristic length scale of sample cell, cm
n = refractive index of the film
n_1 = refractive index of the solvent
n_2 = refractive index of the substrate
N = number of cells in space grid
r = ellipsometric ratio
r_p = Fresnel reflection coefficient parallel to the plane of incidence
r_s = Fresnel reflection coefficient perpendicular to the plane of incidence
S_P = sensitivity to parameter P
t = time, s
V_0 = velocity of injection stream, cm/s
y = ellipsometric measured quantity
z = perpendicular distance from the surface, μm

Greek letters

Γ = surface concentration, mg/cm^2
Γ_m = maximum surface concentration, mg/cm^2
ε_p^r = phase of the electric field component of the reflected wave parallel to the plane of incidence
ε_p^i = phase of the electric field component of the incident wave parallel to the plane of incidence
ε_s^r = phase of the electric field component of the reflected wave perpendicular to the plane of incidence
ε_s^i = phase of the electric field component of the incident wave perpendicular to the plane of incidence
θ = surface coverage
λ = incident beam wavelength, nm
ν = kinematic viscosity of water, cm^2/s
Σ = lateral tension, J/cm^2
Σ_e = line tension, J/cm

Literature Cited

1. Tirrell M, Kokkoli E, Biesalski M. The role of surface science in bioengineered materials. *Surf Sci*. 2000;500:61-83.
2. Berndt P, Fields GB, Tirrell M. Synthetic lipidation of peptides and amino-acids—Monolayer structure and properties. *J Am Chem Soc*. 1995;117:9515-9522.
3. Texter J, Tirrell M. Chemical processing by self-assembly. *AIChE J*. 2001;47:1706-1710.
4. Tirrell M. Modular materials by self-assembly. *AIChE J*. 2005;51: 2386-2390.
5. Kam L, Boxer SG. Formation of supported lipid bilayer composition arrays by controlled mixing and surface capture. *J Am Chem Soc*. 2000;122:12901-12902.
6. Dillow AK, Ochsenhirt SE, McCarthy JB, Fields GB, Tirrell M. Adhesion of alpha(5)beta(1) receptors to biomimetic substrates constructed from peptide amphiphiles. *Biomaterials*. 2001;22:1493-1505.
7. Smith JT, Tomfohr JK, Wells MC, Beebe TP, Kepler TB, Reichert WM. Measurement of cell migration on surface-bound fibronectin gradients. *Langmuir*. 2004;20:8279-8286.
8. Reimhult E, Hook F, Kasemo B. Intact vesicle adsorption and supported biomembrane formation from vesicles in solution: Influence of surface chemistry, vesicle size, temperature, and osmotic pressure. *Langmuir*. 2003;19:1681-1691.
9. Lipowsky R, Seifert U. Adhesion of vesicles and membranes. *Mol Cryst Liq Cryst Sci Technol*. 1991;202:17-25.
10. Salafsky J, Groves JT, Boxer SG. Architecture and function of membrane proteins in planar supported bilayers: A study with photosynthetic reaction centers. *Biochemistry*. 1996;35:14773-14781.
11. Johnson JM, Ha T, Chu S, Boxer SG. Early steps of supported bilayer formation probed by single vesicle fluorescence assays. *Biophys J*. 2002;83:3371-3379.
12. Williams LM, Evans SD, Flynn TM, Marsh A, Knowles PF, Bushby RJ, Boden N. Kinetics of formation of single phospholipid bilayers on self-assembled monolayer supports, as monitored by surface plasmon resonance. *Supramol Sci*. 1997;4:513-517.
13. Keller CA, Glasmastar K, Zhdanov VP, Kasemo B. Formation of supported membranes from vesicles. *Phys Rev Lett*. 2000;84:5443-5446.
14. Koenig BW, Gawrisch K, Krueger S, Orts W, Majkrzak CF, Berk N, Silverton JV. Membrane structure at the solid/water interface studied with neutron reflectivity and atomic force microscopy. *Biophys J*. 1996;70:Wp229-Wp229.
15. Egawa H, Furusawa K. Liposome adhesion on mica surface studied by atomic force microscopy. *Langmuir*. 1999;15:1660-1666.
16. Reviakine I, Brisson A. Formation of supported phospholipid bilayers from unilamellar vesicles investigated by atomic force microscopy. *Langmuir*. 2000;16:1806-1815.
17. Benes M, Billy D, Hermens WT, Hof M. Muscovite (mica) allows the characterisation of supported bilayers by ellipsometry and confocal fluorescence correlation spectroscopy. *Biol Chem*. 2002;383:337-341.
18. Csucs G, Ramsden JJ. Interaction of phospholipid vesicles with smooth metal-oxide surfaces. *Biochim Biophys Acta Biomembr*. 1998; 1369:61-70.
19. Hubbard JB, Silin V, Plant AL. Self assembly driven by hydrophobic interactions at alkanethiol monolayers: Mechanism of formation of hybrid bilayer membranes. *Biophys Chem*. 1998;75:163-176.
20. Zhdanov VP, Keller CA, Glasmastar K, Kasemo B. Simulation of adsorption kinetics of lipid vesicles. *J Chem Phys*. 2000;112:900-909.
21. Petrov JG, Pfohl T, Mohwald H. Ellipsometric chain length dependence of fatty acid Langmuir monolayers. A heads-and-tails model. *J Phys Chem B*. 1999;103:3417-3424.
22. Weaver DR, Pitt WG. Sticking coefficients of adsorbing proteins. *Biomaterials*. 1992;13:577-584.
23. Kucerka N, Kiselev MA, Balgavy P. Determination of bilayer thickness and lipid surface area in unilamellar dimyristoylphosphatidylcholine vesicles from small-angle neutron scattering curves: A comparison of evaluation methods. *Eur Biophys J Biophys Lett*. 2004;33:328-334.
24. Azzam RMA, Bashara NM. *Ellipsometry and Polarized Light*. Amsterdam/New York: North-Holland; 1987.
25. Koenig BW, Kruger S, Orts WJ, Majkrzak CF, Berk NF, Silverton JV, Gawrisch K. Neutron reflectivity and atomic force microscopy studies of a lipid bilayer in water adsorbed to the surface of a silicon single crystal. *Langmuir*. 1996;12:1343-1350.
26. Koenig BW, Strey HH, Gawrisch K. Membrane lateral compressibility determined by NMR and X-ray diffraction: Effect of acyl chain polyunsaturation. *Biophys J*. 1997;73:1954-1966.
27. Lingler S, Rubinstein I, Knoll W, Offenhausser A. Fusion of small unilamellar lipid vesicles to alkanethiol and thiolipid self-assembled monolayers on gold. *Langmuir*. 1997;13:7085-7091.
28. Keller CA, Kasemo B. Surface specific kinetics of lipid vesicle adsorption measured with a quartz crystal microbalance. *Biophys J*. 1998;75:1397-1402.
29. Zheng ZM, Stroumpoulis D, Parra A, Petzold L, Tirrell M. A Monte Carlo simulation study of lipid bilayer formation on hydrophilic substrates from vesicle solutions. *J Chem Phys*. 2006;124:64904.

Manuscript received Apr. 18, 2005, and revision received May 4, 2006.